Durability of an UHPFRC under mechanical and chloride loads

Matos, Ana Mafalda; Chaves Figueiredo, Stefan; Nunes, Sandra; Schlangen, Erik; Barroso-Aguiar, José L.

Important note
To cite this publication, please use the final published version (if applicable).
Please check the document version above.

Durability of an UHPFRC under mechanical and chloride loads

Ana Mafalda Matos [a,*], Stefan Chaves Figueiredo [b,c], Sandra Nunes [a], Erik Schlangen [b], José L. Barroso-Aguiar [d]

[a] CONSTRUCT-LABEST, Faculty of Engineering, University of Porto, Porto, Portugal
[b] MICROLAB, Faculty of Civil Engineering and Geosciences, Delft University of Technology, Delft, the Netherlands
[c] Department of Built Environment, Eindhoven University of Technology, Eindhoven, the Netherlands
[d] Department of Civil Engineering, University of Minho, Centro de Território, Ambiente e Construção, Guimarães, Portugal

ARTICLE INFO

ABSTRACT

The high cost of UHPFRC is a limitation on the practical application in real construction projects. However, a very competitive UHPFRC approach is the hybrid structural elements, where thin layers of UHPFRC are employed to rehabilitate/strengthen damage cover concrete. New layers subjected to harsh conditions (loads and/or environmental) can eventually crack under service conditions, changing the local transport properties and thus, a faster ingress of detrimental substances occur, such as chlorides ions. Most of the studies on chloride penetration in UHPFRC have focused on determining the transport properties of sound, non-cracked specimens. Thus, an experimental campaign was carried out to assess chloride ingress in loaded and/or cracked UHPFRC and the effect of such ions on mechanical performance. Typical service cracks patterns were imposed on UHPFRC specimens and then exposed to wetting–drying cycles in a chloride solution. After 1-year chloride exposure, UHPFRC specimens were in good condition with no significant losses in flexural strength; however, stiffness might be affected. The chloride contents up to 20 mm depth were superior to the European standards critical chloride content. A minimum cover depth of 20 mm of new UHPFRC is recommended to protect a concrete substrate in hybrid structures for exposure classes XS3.

1. Introduction

1.1. Scope

Over the last decades, the efforts to improve the behaviour of cementitious-based materials and the development of the superplasticisers, allowing the efficient disperse of cementitious particles, led to the emergence of Ultra-High Performance Fibre Reinforced Cement-based Composites (UHPFRC). Apart from the fibres fraction, the difference between the cementitious fraction of UHPFRC (so-called UHPC, Ultra high-performance cement-based composite) from ordinary concrete (OC) and even high-performance concrete (HPC) compositions lies mainly in the high cementitious paste volume, cement and supplementary cementitious materials (SCM), usually between (800–1000 kg/m^3), and maximum aggregate dimension, which is limited to 1 mm. The water to binder mass ratio (w/b) is often below 0.20, and consequently, high content of superplasticiser on polycarboxylate ether basis is necessary (in general, 1.4–2.4% by cement weight) [1]. The fibres are, usually, short high-strength steel fibres, which allow incorporating a significant volume (fibre contents ranging, usually, from 2 to 4% in

volume). Besides, the use of special curing treatments (heat treatment, autoclave or steam curing and pressure) is generally applied to UHPFRCs precast elements assembled on-site, such as slender and lightweight elements for pedestrian footbridges and highway bridges, or to build structures with specific architectural or aesthetic requirements [2]. This novel building material provides a unique combination of two essential properties for the structural engineer: extremely low permeability and very high strength [3–7]. A distinguishing feature of UHPFRC is its behaviour under tension.

The high cost of UHPFRC, namely due to some constituent materials and the complexity of the curing processes, is naturally a limitation on the practical application in real construction projects. The use of alternative, more eco and cost-effective materials (as agricultural or industrial waste materials), as well as, standard technology, such as conventional casting and room temperature curing, has been preferred by several authors to promote further applications of UHPFRC [8–10]. Besides, very recently, the concept of Infilled Cementitious Composites (ICC) emerged, consisting of a densely-compacted fibre-aggregate mixture previously optimised and the voids are then filled with a minimal content of cementitious paste [11]. This two-step production concept reduces the paste volume to the minimum while ensuring fibre dispersion, which would not be possible with standard manufacturing.

A very competitive UHPFRC application can be the rehabilitation and strengthening of reinforced concrete structural elements, where small volumes of UHPFRC are needed. The concept of hybrid structures has been applied for the rehabilitation of concrete bridges, in which a new layer of UHPFRC replaces the deteriorated/ cracked older ordinary concrete [12,13]. UHPFRC layer connecting steel girders have also been designed [14] as well as, more recently, the use of UHPFRC in particular zones, such as corroded ends of steel bridge girders or joints [14,15]. Higher structural capacity (stiffness, ultimate strength) and improved durability are expected while keeping compact cross-sectional dimensions. Additionally, advantages are reduced overall construction time and risk, reduced work-force and smaller machinery required. Less environmental impact on the construction site due to shorter-duration temporary work, is also expected [12,16]. Besides, UHPFRC elements require less maintenance due to improved durability, reducing life-cycle cost while yielding much longer service life [12,17–19].

Considering this concept of hybrid structures, controlling the cracking risk of the new layer of UHPFRC, namely at early ages [20], seems crucial for guaranteeing enhanced long-term performance and longer service life. Nevertheless, the magnitude of the internal stresses is influenced by the shrinkage rate and magnitude and the development of material properties during the first ages, namely, tensile creep and the evolution of the young modulus and strength. Indeed, the tensile performance is crucial for handling the typical high autogenous volume change of UHPFRC and acting as almost impermeable layer protection even when subjected to critical tensile strains. So far, numerous studies have evaluated the effect of fibre and cementitious matrix properties on the tensile and flexural behaviours of UHPFRCs. The tensile performance of UHPFRC is considerably affected by the fibre, namely, the fibre content, shape, aspect ratio, distribution and orientation. Tensile performance mostly depends on the fibre-to-matrix bond mechanics [21,22] and the fibre distribution/orientation [23], since the other parameters can be controlled. The fibre distribution/orientation is influenced by the rheology, casting methods, geometry and dimensions of the structural concrete element. Thus, the effective tensile response under real service conditions can differ from that obtained in laboratory conditions, and cracking might occur in the new UHPFRC layer. In some applications, micro-cracked UHPFRC could be subjected to aggressive environments. The unforeseen cracks would allow the ingress of aggressive agents leading to a more rapid deterioration of UHPFRC than it would be expected considering the durability based on the uncracked material [24–27].

In terms of UHPFRC durability, one of the most significant causes of deterioration to be considered is chloride ingress, since bridges rehabilitation is a potential application, which can cause corrosion of steel fibres or steel reinforcement, in the case of reinforced UHPFRC layers. Most of the studies on chloride penetration in UHPFRC have focused on determining sound specimens transport properties. In fact, standard laboratory tests have demonstrated excellent on undamaged UHPC specimens, employing porosity, chloride ion penetration, air penetration and water absorption tests [1,6,28–31]. However, in-service conditions the UHPFRC layers might be micro-cracked, which might change the new covers local transport properties, allowing rapid ingress of chloride ions and the onset of corrosion. Thus, further research is needed on the influence of cracking on UHPFRC resistance to chlorides ingress.

So far, few results on the impact of combined mechanical loading or cracking on the chloride ingress in UHPFRC are available in the literature. The chloride exposure effect was accessed, namely, by means of i) chloride penetration depth [32,33] ii) chloride content at several penetration depths [32–35], including self-healing treatments effects [34,35], iii) mechanical tests after chloride exposure (comparing with virgin specimens) [32,36], and iv) corrosion mitigation of steel rebars [37]. Main conclusions of publications dealing with this subject are described in the following paragraphs.

Real field scenario tests of Thomas et al. [32], in which several types of UHPFRC specimens remained at the mid-tide level of the marine exposure site at Treat Island, revealed that specimens were in excellent condition with no evidence of surface scaling, mass loss or cracking. In terms of chloride attack, the maximum chlorides penetration depth for all specimens ranged approximately from 7 to 12 mm and the chloride content close to specimens surface was roughly 0.20%. Chunping et al. [33] investigated the durability of flexural loaded UHPFRC specimens (w/b = 0.16 and 2% volume of steel fibres) with nano-TiO_2 incorporation. After 90 days of immersin in a 10% NaCl solution, the chloride penetration depth in all UHPC specimens was above 5 mm. Besides, in the first 5 mm of the specimens depth, the chloride concentrations were 0.15%. Similar conclusions were drawn by Ma et al. [34], which exposed UHPFRC specimens (w/b = 0.20 and 2% volume of steel fibres) to a 5% NaCl solution during 7 and 28 days for tensile loaded specimens, and during 28 days for UHPFRC compressive loaded specimens. Concerning tensile loaded specimens, the maximum chloride content decreases with the increase of penetration depth, and it increases with the increase of applied load and chloride penetration time. When the tensile stress applied was above 50% of ultimate tensile stress, more cracks passageways allowed the chloride water solution penetrate deeper into UHPFRC. In brief, the maximum chloride content was 0.143%, 0.165%, 0.383% and 0.502% after 28 days chloride exposure, for 0%, 30%, 50% and 80% of ultimate tensile stress, respectively. The increase of compressive loading also provided an increase in the chloride content penetrated. The maximum chloride content of UHPFRC loaded with 0%, 30%, 50% and 80% of ultimate compressive strength was 0.156%, 0.351%, 0.430% and 0.466%, respectively. Wittmann et al. [35] studied the influence of several tensile loading (30, 50, and 80% of the tensile strength) on chloride penetration in UHPFRC (w/b = 0.20 and 2.0% volume of steel fibres). Besides, specimens with the same loading damage were also tested in the unloaded state and non-damage specimens. Chloride capillary absorption under imposed constant strain was performed using a box of 40×100 mm^2 fixed to the surface of the specimen. The capillary penetration of 5% NaCl solution was performed for 28 days. Non-damage specimens absorbed fewer chlorides (0.139% at specimens surface), and the content became very low after 2.5 mm depth. Under tensile load, the chloride ingress slightly increased for tensile stresses corresponding to 30% of the tensile strength (from 0.233 at surface to 0.034% at 15 mm of depth). In case the higher stress, 50% and 80% of the tensile strength, substantial amounts of chloride penetrated the specimens, 0.514% and 0.723% at specimens surface, respectively, presenting a still significant amount of chlorides up to 9.5 mm depth, 0.064% and 0.139%, respectively. For the same load levels, but tested in an unloaded state, a lower content of chlorides penetrated

in UHPFRC specimens.

Healing treatments after cracking occurrence can also influence chloride ingress. In fact, self-healing may be a protective system of concrete structures against chloride-rich environments, such as marine environments [38]. The healing ability of UHPFRC, namely in the case of microcracking, is responsible for the recovery of both durability properties (water permeability, immersion or wet dry cycles in geothermal water) and mechanical performance, as stated in previous research works of Cuenca et al. [39], Cuenca and Serna [40], Cuenca et al. [41]. This also occurred when UHPFRC was exposed to a chloride-rich environment, as stated by Thomas et al. [32], which concluded that several types of UHPFRCs mechanical performance remained intact after 7–12 years of "on site" marine exposure. Parant et al. [36] also concluded that the mechanical properties, strength and stiffness, of UHPFRC were not compromised after chloride aggressive environment exposure and/or loading. Ma et al. [34] and Wittmann et al. [35] treated cracked UHPFEC specimens on a saturated $Ca(OH)_2$ solution before chlorides exposure and observed that the maximum chloride content of UHPFRC after exposure to the self-healing treatment decreased. El-Joukhadar and Pantazopoulou [37] investigate the efficiency of few types of UHPFRC in mitigating reinforcement corrosion when exposed to chloride environments. One of the major findings was that these materials were able to mitigate corrosion in the absence of service cracks fully. Even though the effectiveness of rebar protection was gradually reduced with increasing crack width, UHPFRC was a much more effective barrier against corrosion than conventional concrete.

1.2. Research objectives

Recently the authors developed a new UHPFRC mixture using locally available raw materials (Portugal/Europe). This mixture aimed to be functional to rehabilitation applications (without special curing treatments) and able to be cast on-site (self-compacting). It was also optimised in terms of early-age autogenous shrinkage, durability, cost and eco-efficiency (lower cement + silica fume contents and incorporating a waste material from Portuguese oil refinery) [29].

An evaluation of several durability indicators of new developed UHPC (without steel fibres) to determine the resistance against various aggressive agents was conducted in a previous study [42,43,58], and results of durability indicators show that new UHPC presents very high durability compared to OC and even HPC. Besides, it corroborates the range of durability parameters found in the literature for other UHPFRC [42,43,58]. The experimental characterisation of the capillary transport properties on cracked and non-cracked UHPFRC, with different fibre dosages, was also presented in previous work [44], and it showed its excellent tightness to water.

However, it is needed to determine whether this UHPFRC retains its long-term durability when exposed to chlorides after cracking under service conditions. The current paper addresses the chlorides ingress in non-cracked, cracked-unloaded and cracked-loaded UHPFRC specimens, with a typical fibre content of 3.0%. Several damage levels were induced on UHPFRC specimens, the crack pattern was characterised, and then the specimens were subjected to wetting–drying cycles, using a concentrated chloride solution (3.5% NaCl), during 1 year. Afterwards, several parameters were evaluated, namely, mechanical performance, chloride penetration depth and chloride content.

2. Experimental programme

2.1. Raw materials and mix proportions

A ternary UHPFRC binder mixture was employed, constituted by, CEM I 42.5R Portland cement complying with EN 197-1 [45], and as SCM silica fume and limestone filler complying with the requirements of EN 13263-1 and EN 12620, respectively. The aggregate fraction is constituted by 85% siliceous natural sand (0–1 mm) and 15% of spent

Table 1
UHPFRC mixture composition.

Raw materials		(kg/m^3)
Binder phase	Cement	690.2
	Silica fume	33.6
	Limestone filler	250.6
Aggregates	ECat	155.5
	Siliceous sand	775.0
Admixture	Superplasticizer	19.5
Reinforcement	Steel fibres	235.0
Water	Mixing water	160.9
	ECats absorption water	46.6

Table 2
Mixing sequence.

Steps	Duration	Speed
Add ECat (dry state) with 80% mixing water plus the ECat water absorption	5.0 min	140 ± 5 rotations·min^{-1}
Add cement + limestone filler + silica fume + sand and mix	2.5 min	
Mix	2.5 min	
Add the rest of the water plus 75% of Sp and mix	2.5 min	
Add the rest of Sp and mix	1.5 min	
Add fibres and mix	2.0 min	

equilibrium catalyst (ECat). In brief, ECat consists on waste material from the oil industry and is available in Portugal. Besides other exciting properties to be applied in cement-based materials [29], the high specific surface (150 070 m^2/Kg) with high water absorption (30%, by mass), made up the idea to be used as an internal curing agent mitigating the UHPFRC autogenous shrinkage [29]. It was, then, necessary to add extra water for ECat absorption during mixing (see Table 1). A polycarboxylate superplasticiser with a specific gravity of 1080 Kg/m3 and 40% solid content and potable water was included. As reinforcement, 3.0% by volume of smooth short steel fibres, with 13 mm length and 0.21 mm diameter, and 2750 MPa of tensile strength, were used. More details concerning raw materials origin and properties can be found elsewhere [29]. Table 1 presents the mixture proportions of the new UHPFRC.

2.2. Specimens preparation and curing

A mixer as specified in NP EN 196–1 was employed to manufacture UHPFRC mixtures. The mixing procedure followed the steps described in Table 2. The number of specimens produced for each condition is detailed in Table 3. After demolding, 24 h later, specimens were water cured in a fog room at 20 ± 2 °C until the testing age.

The referencing of specimens considered the fibre content, the target COD and the specimen replicate number. For example, "3.0%-350–1", corresponds to a specimen (replica) number one, incorporating 3.0% steel fibres and a target COD_{load} of 350 µm. Specimens for flexural strength assessment were named as "3.0%-W28-i" and "3.0%-W379-i" corresponding to water curing time of 28 and 379 days, respectively.

2.3. Mechanical testing

Flexural strength through a four-point bending test of UHPFRCs 40x40x160 mm^3 specimens was assessed at 28 and 379 days for water cured specimens and 138 and 379 days for samples exposed to chlorides (see Table 3). The device for applying loads is depicted in see Fig. 1. Dimensions and proportions of specimens and load application were adjusted according to EN 12390–5, in which distance between loading point is d, being d the width of the specimen (40 mm in this case) and span is $3d$, as illustrated in Fig. 1. The flexural strength in MPa (f_{cf}) can

Table 3
Detailed experimental programme including: number of prismatic specimens prepared for each test condition.

Specimens reference	Number of specimens	Conditioning before cracking	Cracking age	Target COD_{load}	Testing age	Outcomes
Four-point bending tests						
3.0%-W28d-i	5	Immersion in water at 20 °C up to 28 d	–	–	28 d	Load-displacement curves at 28 d
3.0%-W379d-i	5	Immersion in water at 20 °C up to 379 d	–	–	379 d	Load-displacement curves at 379 d
Exposure to wetting–drying cycles (3.5% NaCl water solution, 20 °C) after cracking at 28 d						
3.0%-0-i(non-cracked and exposed to chlorides)	5	Immersion in water at 20 °C up to 28 d	28 d	0 µm	379 d	Load-displacement curves after wetting drying cycles Chlorides profile Chloride penetration depth
3.0%-300-i (exposed to chlorides in loaded state)	2		28 d	300 µm	138 d	Load-displacement curves after wetting drying cycles Chloride profileChloride penetration depth
	2					
	3				379 d	Load-displacement curves after wetting drying cycles Chloride profileChloride penetration depth
	2					
3.0%-350-i(exposed to chlorides in unloaded state)	5		28	350 µm	379 d	Load-displacement curves after wetting drying cycles Number of cracks and crack widthsChloride profileChloride penetration depth
	3					
3.0%-400-i(exposed to chlorides in unloaded state)	5		28 d	400 µm	379 d	Load-displacement curves after wetting drying cycles Number of cracks and crack widthsChloride profileChloride penetration depth
	3					

Fig. 1. Four-point bending test.

be calculated from the maximum load sustained (*F*) as follows:

$$f_{cf} = \frac{Fmax \times I}{d_1 \times d_2{}^2} \tag{1}$$

Where *I*is the span (mm), d_1 and d_2 are the width and depth of the test beam (mm), respectively.

2.4. Cracking methodology

The authors previously established the cracking methodology, and detailed information can be consulted in [44]. After 28 days of water curing, prismatic specimens were cracked by imposing different crack open displacements (COD), namely, 300, 350 and 400 µm, considering possible service conditions and obtaining different crack patterns. Detailed information concerning the number of specimens used for each test condition is indicated in Table 3. Two LVDTs, fixed at each specimens front and back surfaces, perpendicular to the loading direction, were used to real-time monitor the COD while loading, as depicted in Fig. 1. A 300 kN Instron testing machine controlled the displacement rate during the experiment, which was 0.003 mm/s. When the target COD was achieved (COD_{load}), the specimens "3.0%-350-i" and "3.0%-400-i" were unloaded, and these specimens were with residual COD (COD_{res}) only. Then, the cracks pattern was observed in the tensile face

of these specimens and characterised according to the procedure described in section 2.5. Meanwhile, specimens were stored in the testing room at 20 °C ± 2 and RH = 50 ± 5% during seven days before starting the chloride cycles described in section 2.6.

"3.0%-300-i" specimens, i.e., predefined COD_{load} = 300 µm, were subjected to chloride rich environment under loading. For that purpose, a stainless-steel frame designed by the authors was used to keep the COD_{load}. The specimens were unloaded, but LVDTs were not removed while they were allocated on a stainless-steel frame, as shown in Fig. 2. The specimens were then re-loaded up to COD_{load} of 300 µm using threaded rods tightened by a torque wrench. Conserving the LVDTs on the specimen allowed achieving the target COD again. Afterwards, LVDTs were removed prudently, and the frame sustained the target COD. Thus, "3.0%-300-i" specimens were subject to wetting–drying chlorides cycles in a loaded state.

Before initiating the wetting–drying cycles, all prisms side and compression surfaces were sealed using waterproof tape to ensure the chloride penetration only through the cracked surface, as can be seen in Figs. 2 and 3. It must be noted that it was impossible to protect the loaded surfaces of specimens kept in the stainless-steel frame (3.0%-300-i).

2.5. Crack number and crack width measurements

After 28 days water curing, a matrix was marked on the tensile face of some specimens of each COD group (40 mm, in between the two loading points) as shown in Fig. 3 and detailed in Fig. 4 and Table 4. This aimed to simplify the crack pattern characterisation (width and numbering) since in UHPFRC usually, multiple cracking occurs before reaching peak load. The matrix is formed by three horizontal lines (A, B and C, shown in Fig. 4 and Table 4) and 4 columns (segments 1, 2, 3 and 4, shown in Fig. 4 and Table 4). All cracks crossing the lines (A, B or C) were counted and measured. Thus, in each quadrant (1, 2, 3 or 4) there is N $_{i…n}$ cracks (see Table 4).

The crack number and width were observed and measured utilising a Microscope Multizoom Nikon AZ100 with an objective Nikon-AZ Plan Fluor 5 × and photographed with a PC and a DS-U2 digital camera. An example of a photo of a crack is shown in Fig. 5. Six crack-width measurements were performed for each crack crossing lines A, B or C, as exemplified in Fig. 5, using image analysis software (ImageJ). Each crack is represented by the median of crack with (see the scheme of Table 4 and measures on Fig. 18). On loaded specimens, kept inside the frame, it was impossible to perform the crack pattern characterisation.
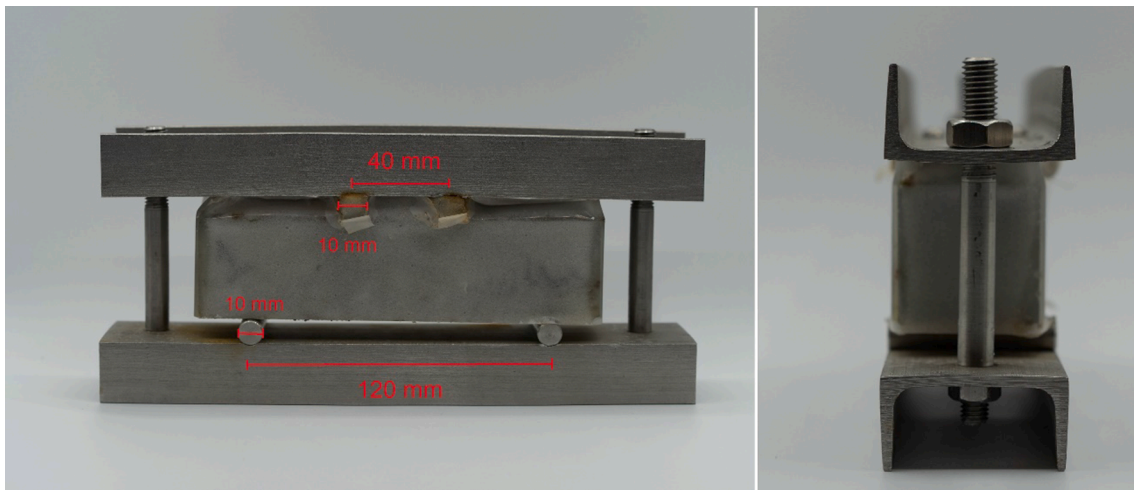
Fig. 2. Illustration of the loading device.
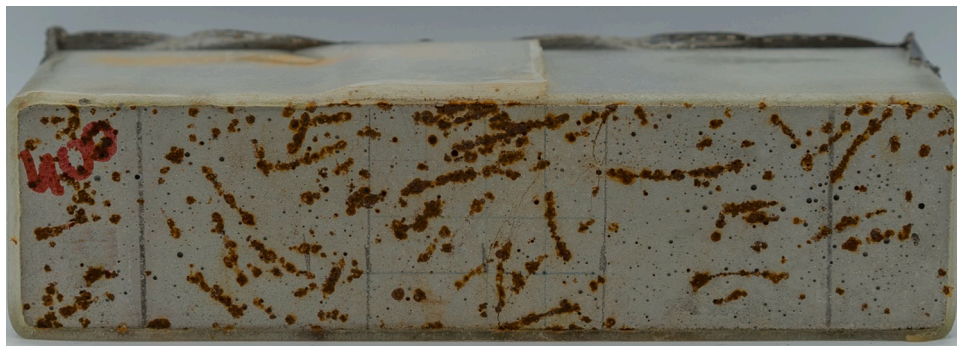
Fig. 3. Tensile surface of specimen "3.0%-400–5" after cracking.
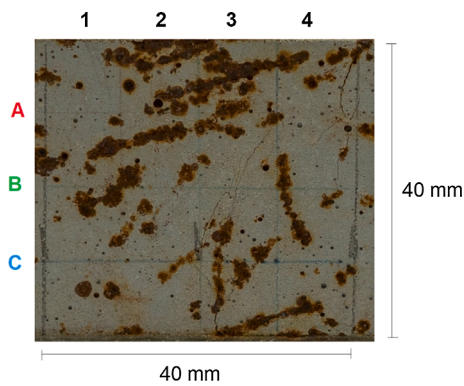
Fig. 4. Schematic matrix for crack opening measurement, the specimen "3.0%-400–5".
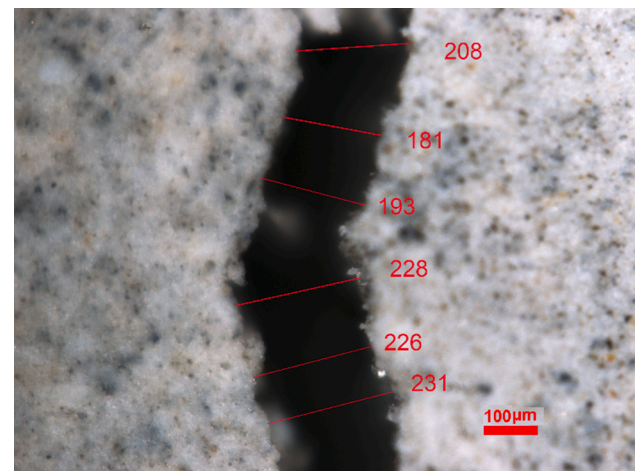
Fig. 5. Typical photo made from the measurement of one crack width (specimen "3.0%-400–5", localisation in the matrix: A-4).

Table 4
Crack number and crack width schematic matrix (Matrixes available at Appendix B and C).

	1	2	3	4
A	Crack width (N_i… $_n$)	Crack width (N_i… $_n$)	Crack width (N_i… $_n$)	Crack width (N_i… $_n$)
B	Crack width (N_i… $_n$)	Crack width (N_i… $_n$)	Crack width (N_i… $_n$)	Crack width (N_i… $_n$)
C	Crack width (N_i… $_n$)	Crack width (N_i… $_n$)	Crack width (N_i… $_n$)	Crack width (N_i… $_n$)
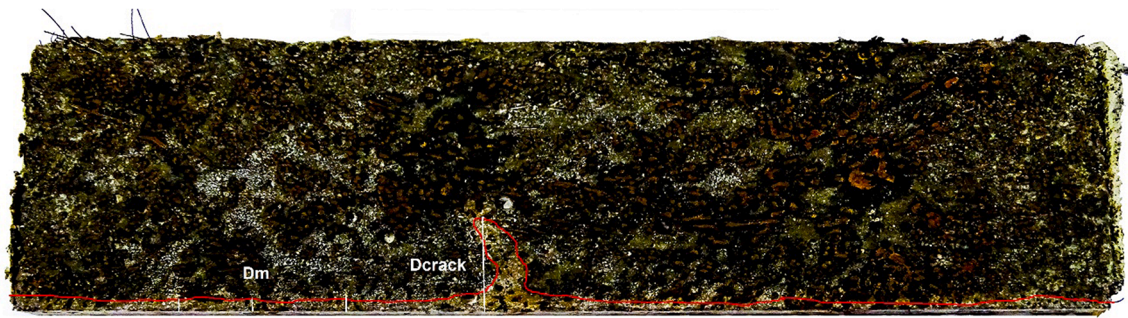
Fig. 6. Chloride penetration profiles on a cracked specimen ("3.0%-350-5").
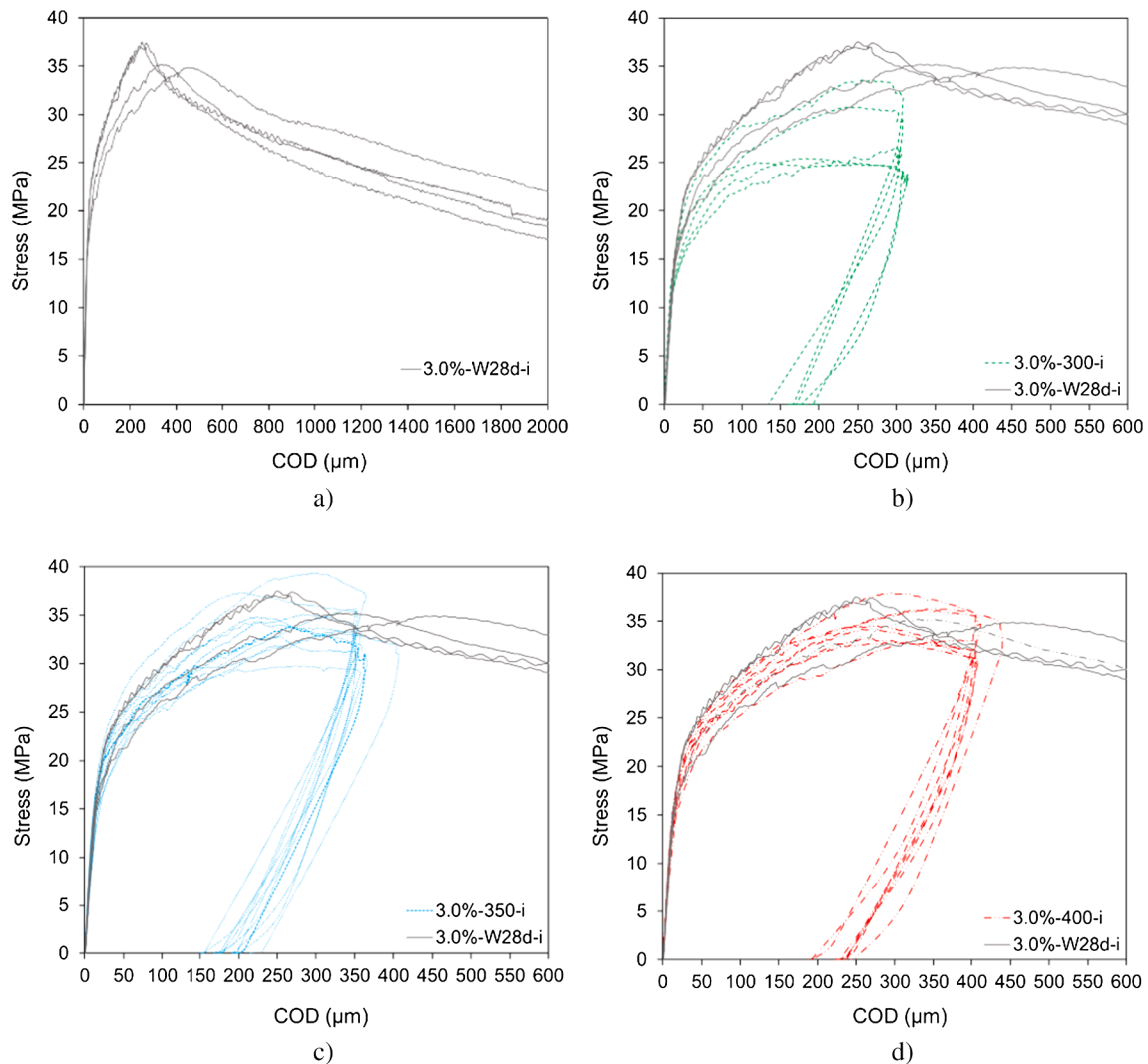
Fig. 7. a) Four-point bending load–displacement relationship after 28 days of wet curing and Load-displacement curves obtained at 28 days while establishing target CODs: b) COD_{load} = 300 μm, c) COD_{load} = 350 μm and d) COD_{load} = 400 μm.

2.6. Exposure to chloride rich environment

For the long-term chloride experiment the "3.0%-0-i" (non-cracked), "3.0%-300-i" (loaded, kept in stainless steel frame), "3.0%-350-i" and "3.0%-400-i" (unloaded, with residual cracks) specimens were tested, as described in Table 3. As mentioned before, all UHPFRC specimens side surfaces were sealed to ensure the chloride penetration only through the cracked surface. The specimens tensile surfaces were exposed to chlorides by partially immersing the specimens in a chloride solution simulating seawater (3.5% NaCl). The specimens were subjected to a weekly based wetting–drying cycle consisting of two days of partial immersion and five days of drying at 20 °C and RH = 50%. Most specimens were exposed to chloride cycles during 379 days. In the case of "3.0%-300–1", "3.0%-300–2", "3.0%-300–3" and "3.0%-300–4" specimens, the wetting–drying cycles were stopped after 138 days (see Tables 3 and 7 of Appendix B) for an earlier assessment of the chlorides penetration in UHPFRC, as well as, the four-point flexural behaviour.
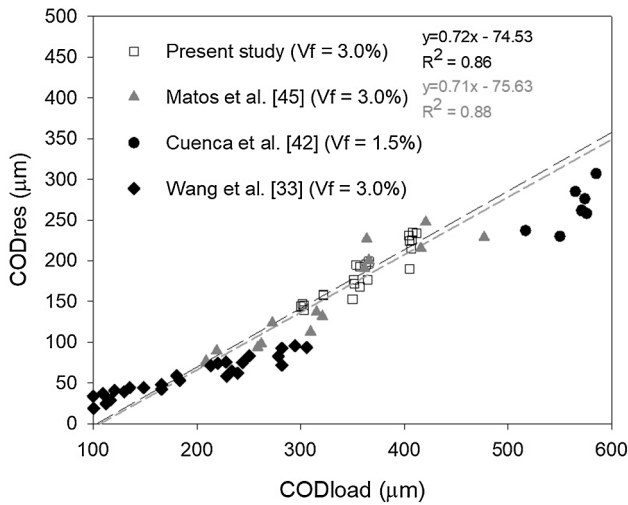
Fig. 8. Relation between COD_{load} and COD_{res}.

2.7. Chloride penetration depth and chloride content

After the chloride exposure described in section 2.6, some specimens were used to assess chloride penetration depth and the chloride content

(see details in Table 3). To avoid chlorides ions leaching, a dry cut method was employed to split the specimens longitudinally. One part of each specimen was used to check chloride penetration depth by spraying a 0.1 M silver nitrate solution on the cut surface, as illustrated in Fig. 6.

The other half of each cut specimen was used to determine the chloride content. Thus, powder samples were taken from the central part of the specimen (in between the two load points) in the direction of chloride penetration on a cracked and non-cracked area following the "dry drilling method" sampling procedure described in RILEM Recommendation TC 178-TMC [46]. Powdered samples corresponding to depth steps of approximately 5 mm up to 20 mm of specimen depth were obtained. The steel fibres were removed from the powder sample using a magnet. As a reference, the initial chloride content (C_0) was determined on a specimen not exposed to chlorides, following the same procedure and at the same depths. The determination of chlorides content followed the procedure described in NP EN 196-2 [47], which gives the total chloride content expressed as chloride ion (Cl^-) by mass of sample without fibres (UHPC).

3. Experimental results and discussion

3.1. Crack pattern characterisation

3.1.1. COD after unloading (COD_{load} and COD_{res})
Figure 7-b, -c and -d depict the load–displacement curves obtained

a)

b)

c)
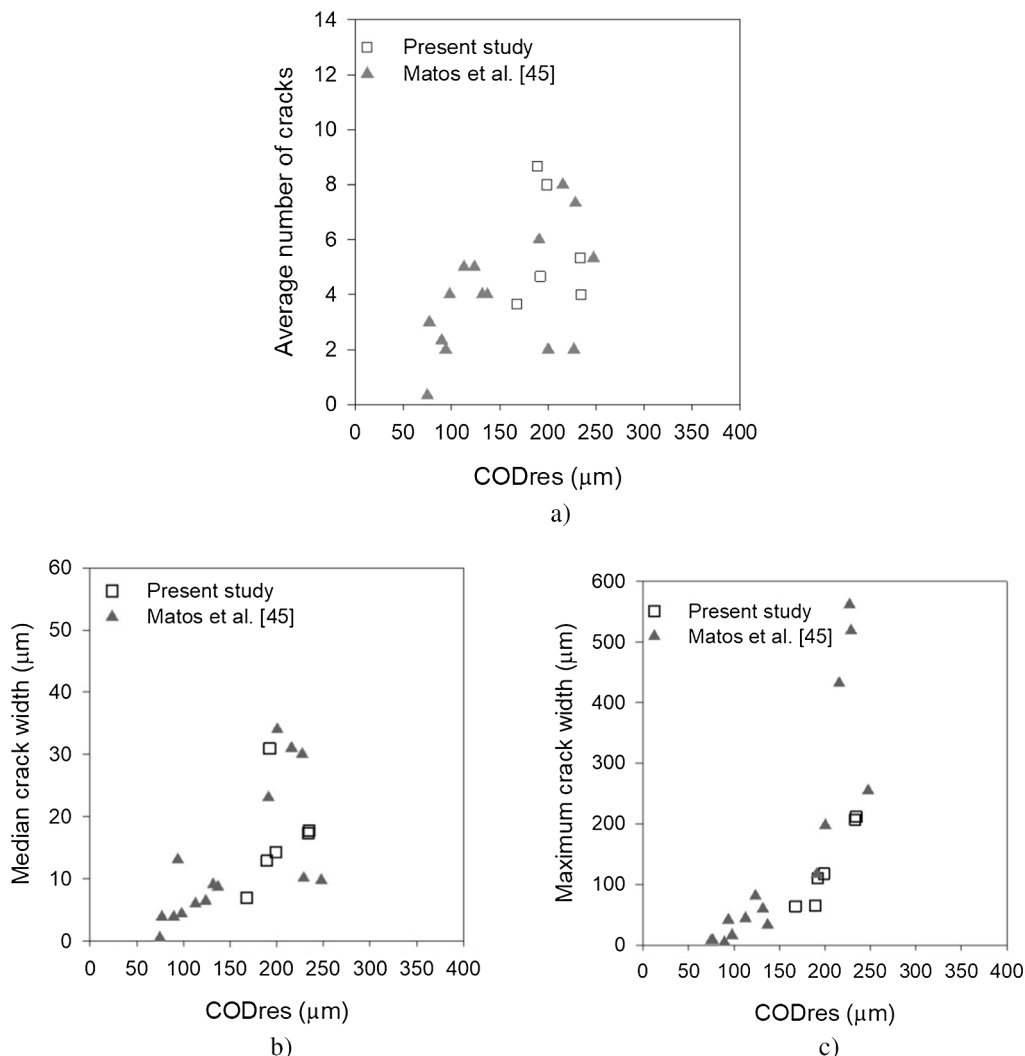
Fig. 9. Crack pattern parameters: a) Average number of cracks over 40 mm; b) Median crack width; c) Maximum crack width.

Fig. 10. Multiple micro-cracking formations in flexural harding stage (micro-cracks revealed by alcohol spayed on the surface).

Fig. 11. Macro crack formation in softening stage (valid result).

while establishing target $COD_{load\ and}$ the curves of specimens tested under four-point bending up to the beginning of softening region, at 28 days (grey lines). These curves are also depicted in Fig. 7-a up to the end of the test. As can be seen, the goal values of COD_{load} were reached with a rational approximation ($\pm15\%$) concerning all tested specimens. Table 7 in Appendix B presents data regarding each specimens main cracking parameters, i.e., maximum load achieved during the cracking procedure (Fcr, max) and the values of COD_{load} and COD_{res}. COD_{res} obtained after unloading as a function of COD_{load} are represented in Fig. 8, showing a significant linear relationship between these two parameters. This trend corroborates with previous studies [30,39] and also with previous studies carried out by the authors [44], which were also dipicted in the Fig. 8.

3.1.2. Crack pattern

Crack matrices of every single specimen (with each crack width median in μm) are presented in Appendix A. The grading colour scale between green and red adopted in that matrices, in which green represents tinner cracks and ref the wider, allows easy comprehension of crack open dimension. In addition, the summary of crack pattern parameters, namely, the average number of cracks counted over lines A, B and C (N), the median (Med), minimum (Min) and maximum (Max) crack width and are listed in Table 7 of Appendix B.

Figure 10 presents some attempts to correlate crack parameters with COD_{res} obtained in this study (gry marks). Besides, results from the authors previous study are also depicted in Fig. 9 (triangle marks) [44]. As shown in Fig. 9-a, no clear tendency was found between the number of cracks and COD_{res}. Besides, some remarks must be noted. The average number of cracks observed over a length of 40 mm remained below 9. Concerning the crack open, the crack widths median was below 32 μm, and Fig. 9-b suggested they slightly increase with the damage level. These results agree with the authors previous findings (red marks in Fig. 9) [44]. Fig. 9-c represents the relation between the maximum crack width results with COD_{res}, and it can be drawn that: up to a COD_{res} of about 200 μm, the maximum crack width remained below 75 μm; and a more significant increase of maximum crack width (>200 μm), indicative of macro-crack formation, occurs for higher COD_{res}.
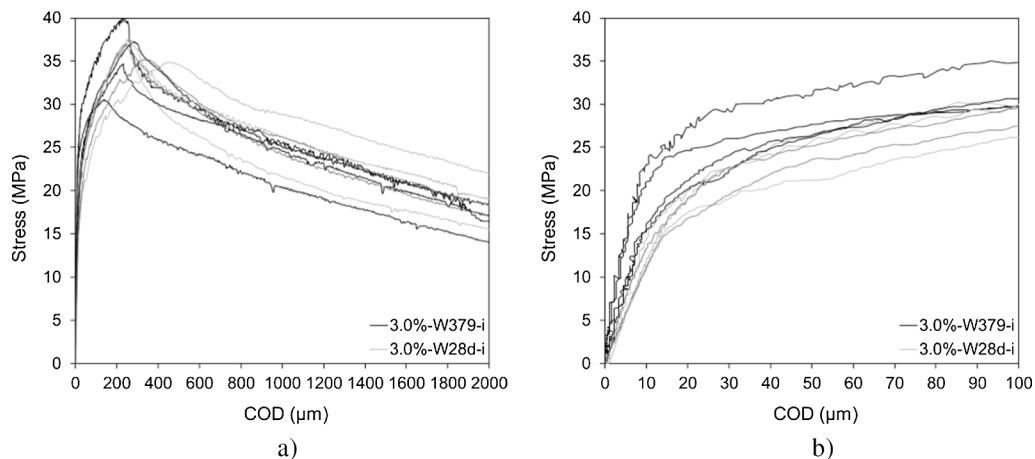
Fig. 12. a) Four-point bending load–displacement relationships for 28 and 379 old days up to softening area and b) Load-displacement curves zoom up to COD = 100 μm.

Table 5
Bending test results summary.

Ref.	N° of specimens	Testing age (days)	F_{max}(kN)	Stress (MPa)	COD_{Fmax}(µm)
3.0% – W_{28}-i	4	28	19.3 ± 0.6	36.2 ± 1.3	325 ± 93
3.0% – W_{379}-i	5	379	19.1 ± 1.7	35.9 ± 3.5	225 ± 51
3.0% – 0 -i (non-cracked)	4	379	21.3 ± 1.7	39.9 ± 3.7	275 ± 47
3.0% − 300-i (exposed to chlorides in loaded state 138 d)*	2	138	23.5 ± 2.1	44.4 ± 2.0	174*
3.0% − 300-i (exposed to chlorides in loaded state)	3	379	18.2 ± 2.2	34.7 ± 5.0	213 ± 91
3.0% − 350-i (exposed to chlorides in unloaded state)	5	379	19.8 ± 0.5	37.1 ± 1.1	255 ± 41
3.0% − 400-i (exposed to chlorides in unloaded state)	5	379	19.0 ± 0.9	36.6 ± 1.9	277 ± 47

* One specimen presented the crack localised outside the measuring length covered by the LVDTs

Table 6
Bending results summary for water cured specimens.

	Specimen	Curing	Testing age (d)	Fmax (kN)	COD_{Fmax} (µm)
3.0% – W28	1	28 days water curing	28	18.62	454
	2			18.78	331
	3			20.00	249
	4			19.74	265
3.0% – W379	1	379 days water curing	379	16.28	139
	2			21.36	237
	3			19.68	238
	4			18.52	231
	5			19.88	278

3.2. Bending behaviour

3.2.1. Water cured specimens

The individual load–displacement curves for all the valid UHPFRC specimens are presented in Fig. 12. A valid result was considered when, after peak loaded is reached, the macro-crack occurs inside the measuring length covered by the LVDTs (exemplified in Fig. 11). For each testing age, 28 and 379 days, five specimens were tested, and valid four and five were considered valid results, for 28 and 379 days, respectively. Average results, i.e., average peak load (F_{max}), Strenght (Stress) and COD at F_{max} (COD_{Fmax}) are summarised in Table 5 (2nd and 3rd lines for "3.0%-W28-i" and "3.0%-W379-i" specimens, respectively) and Table 6 of Appendix B, which contains detailed results. As shown in Fig. 12, flexural hardening behaviour occurred in UHPFRC mixtures with 3% steel fibres.

Before the peak load is reached, i.e., the flexural hardening stage, multiple cracking formations occur, not visible to human eyes, without the appearance of any significant visible crack, as depicted in Fig. 10. A macro-crack forms after the peak load, i.e., the softening stage begin, as illustrated in Fig. 11. The average peak forces F_{max} achieved after 28 and 379 days of water curing were 19.3 ± 0.6 and 19.1 ± 1.7 kN, respectively. Usually, when higher peak stresses are reached, more brittle behaviour in the softening region occurs (lower post-peak ductility) [48]. Fig. 12-b shows that some of the "3.0%-W379-i" specimens exhibit higher initial stiffness, which might be due to further microstructure development with increasing curing time.

3.2.2. Specimens exposed to chlorides

After wetting-drying cycles, the specimens "3.0%-300-i" was removed from the frame and kept at 20 °C and HR = 65% controlled environment for one week before being re-loaded to failure under four-point bending test. The remaining specimens, 3.0%-0-i, 3%-350-i, 3%-400-i, were also kept in the same conditions for one week before mechanical tests. Fig. 13 presents curves of re-loading to failure for the different tested series.

Table 5 summarises the average results for each set of specimens (F_{max}, Stress and COD_{Fmax}), and Table 7 of Appendix B reports the individual results. The comparison of the specimens flexural behaviours shows the following points:

- Non-cracked specimens ("3.0%-0-i") showed similar average peak loads to the cracked specimens (see Fig. 13-a); however, their initial stiffness is, in general, higher (see Fig. 13-b).
- Cracked-loaded specimens (3.0%-300-i) presented similar or improved bending behaviour compared to "3.0%-0-i" specimens,
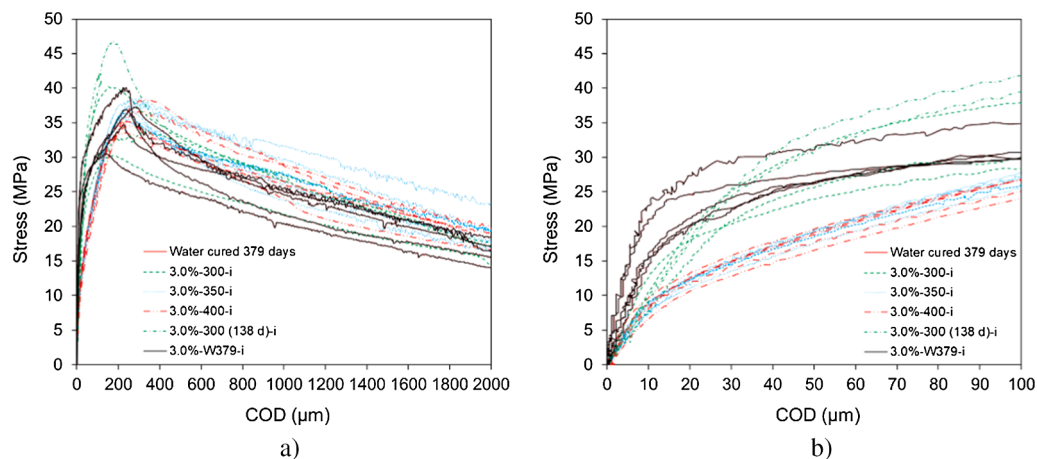
Fig. 13. a) Four-point load–displacement relationships for all valid specimens tested at the end of chlorides cycles and b) Load-displacement curves zoom up to COD = 100 µm.

Table 7
Results summary for specimens exposed to chlorides.

Specimens	N	Crack width (μm)			Cracking parameters				Mechanical properties after long term chlorides exposure		Chloride content (%)				Chloride penetration depth (mm)	
		Median	Min	Max	CODload (μm)	CODres (μm)	CODres tested (μm)	Fcr, max (kN)	Fmax (kN)	COD_Fmax (μm)	0–5 mm	5–10 mm	10–15 mm	15–20 mm	Max Crack zone	Non crack zone
3.0% – 0–1**											0.45	0.08	0.02	–		1.8
3.0% – 0–2									23.33	341	0.79	0.26	0.28	0.29		2.6
3.0% – 0–3									20.21	257	0.53	0.31	0.30	0.24		2.2
3.0% – 0–4									22.57	271	0.57	0.41	0.34	0.31		1.9
3.0% – 0–5									19.05	232	0.47	0.30	0.23	0.21		2.6
3.0% – 300–1**					300	144	300	16.19			0.62	0.44	0.23	0.20		
3.0% – 300–2**					302	147	300	17.86			0.43	0.44	0.27	–		
3.0% – 300–3**					322	157	300	19.14	24.96	174						
3.0% – 300–4**					303	145	300	18.41	22.00	*						
3.0% – 300–5					300	144	300	16.19	17.97	317						
3.0% – 300–6					302	147	300	17.86	16.13	170						
3.0% – 300–7					322	158	300	19.14	21.43	152						
3.0% – 300–8					303	139	300	18.41			0.65	0.38	0.26	0.21	17.50	1.94
3.0% – 300–9					303	145	300	18.41			0.61	0.46	0.21	0.20	18.55	1.51
3.0% – 350–1					363	195	195	17.99	19.16	233						
3.0% – 350–2					351	177	177	18.58	20.53	304						
3.0% – 350–3					352	172	172	17.47	19.16	210						
3.0% – 350–4	5	31	4	110	357	192	192	15.86			0.98	0.60	0.40	0.35	14.1	2.8
3.0% – 350–5	4	7	3	64	357	168	168	18.71			0.61	0.41	0.25	0.25	11.0	2.6
3.0% – 350–6	8	14	3	117	366	199	199	18.31			0.85	0.49	0.29	0.15	13.2	2.6
3.0% – 350–7					354	195	195	19.92	20.18	291						
3.0% – 350–8					365	177	177	20.97			0.74	0.41	0.23	0.21	14.1	1.6
3.0% – 350–9					350	153	153	17.81	19.78	236						
3.0% – 400–1					405	190	190	17.60	20.42	334						
3.0% – 400–2					405	224	224	17.53	18.78	243						
3.0% – 400–3	5	17	2	206	412	233	233	19.26			0.90	0.47	0.19	0.18	14.7	2.1
3.0% – 400–4	9	13	2	65	405	190	190	19.36			0.62	0.41	0.22	0.17	10.5	2.7
3.0% – 400–5	4	18	3	212	408	234	234	17.71			0.88	0.49	0.32	0.19	16.8	2.5
3.0% – 400–6					407	226	226	18.26	17.88	227						
3.0% – 400–7					404	231	231	18.42	18.43	262						
3.0% – 400–8					407	215	215	17.63	19.55	320						

* Crack out of LVDTs range.
** Tested after 138 days of chloride exposure
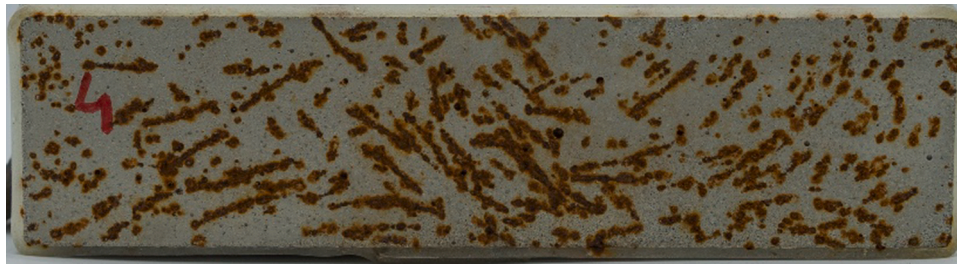
Fig. 14. Exposed specimen surface after wetting–drying cycles (3.0%-0–4).
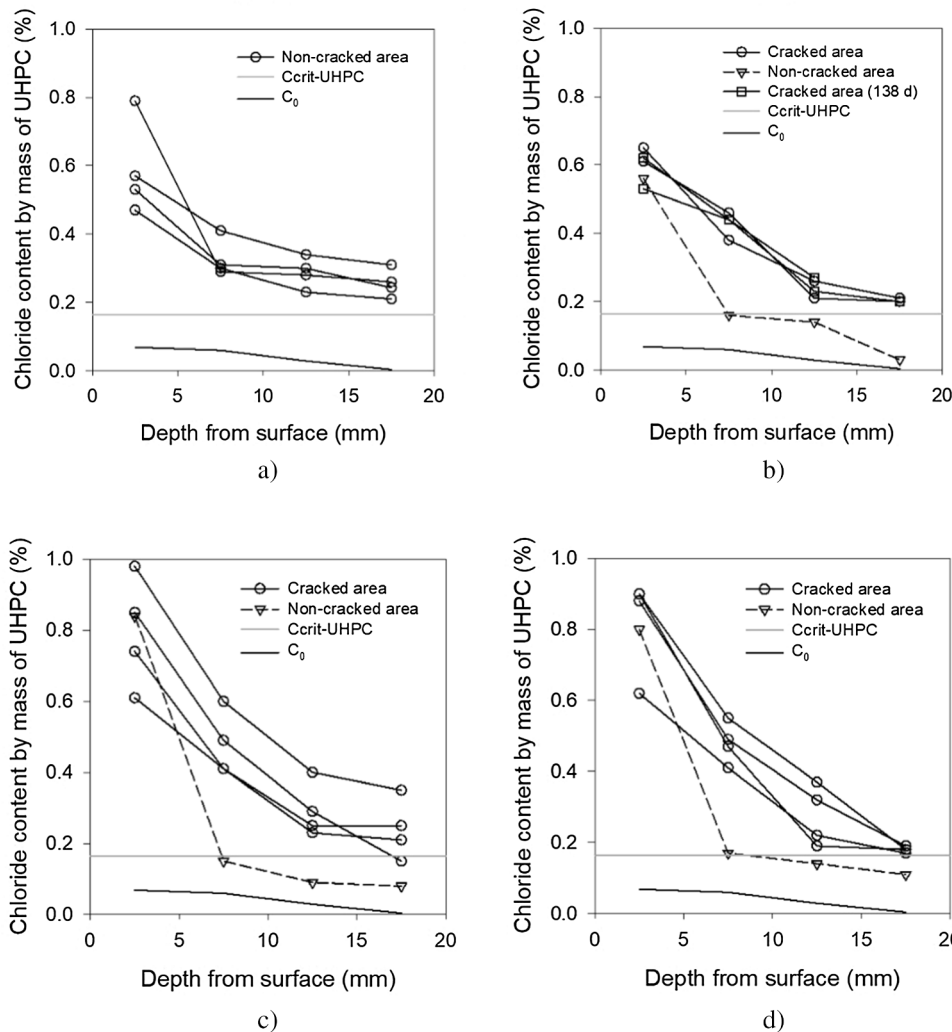
Fig. 15. Chloride profiles for UHPFRC series: a) 3.0%-0-i; b) 3.0%-300-i; c) 3.0%-350-i and d) 3.0%-400-i specimens;

both in terms of peak load (see Fig. 13-a) and initial stiffness (see Fig. 12-b).

- Cracked-unloaded specimens "3.0%-350-i" and "3.0%-400-i" showed similar average peak loads (see Fig. 13-a) but lower stiffness compared to "3.0%-0-i" specimens (see Fig. 12-b).

In cracked UHPFRC specimens, the phenomenon of autogenous healing of cracks could be anticipated due to the very fine crack widths, as also observed in previous research studies [39–41], due to a large amount of anhydrous clinkers available and the presence of wetting--drying cycles [36] . Results presented in Fig. 12 clearly show the autogenous healing of cracks was more pronounced in "3.0%-300-i" specimens compared to other cracked specimens ("3.0%-350-i" and

"3.0%-400-i"), and this self-healing occurred under tensile loading. Similar findings were reported by Parant et al. [36]. This improved behaviour of the "3.0%-300-i" specimens cracked up to $COD_{load} = 300$ μm, and maintained loaded in an aggressive environment, can be explained by the lower damage imposed to these specimens, leading to the formation of only fine microcracks (as reported by the authors in [44]). On the contrary, in the case of "3.0%-350-i" and "3.0%-400-i" specimens, a macro-crack has formed (as evidenced by maximum crack width results reported in Fig. 18 of Appendix A and photos shown in Appendix C), which could not be completely sealed by the autogenous healing, as observed in [37], thus causing an irreversible decrease in the initial stiffness.
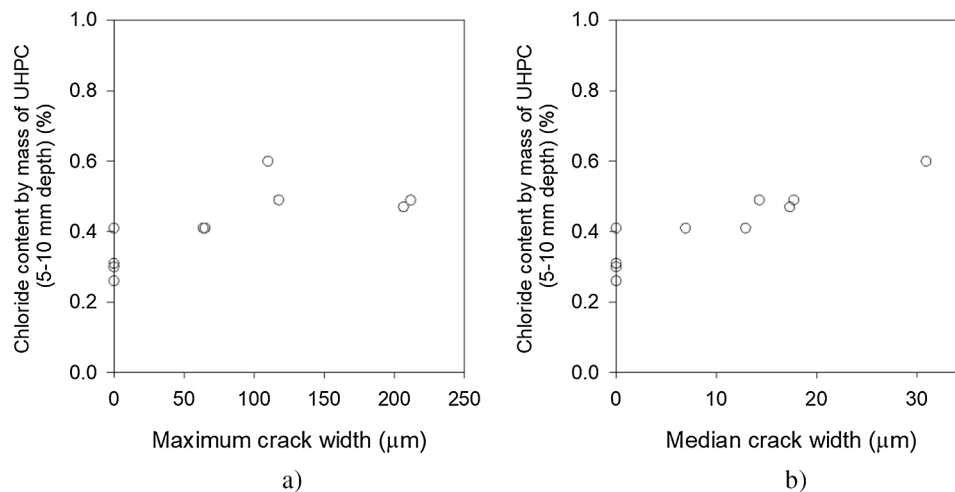
Fig. 16. Relationship between chloride content (5–10 mm depth) on a) maximum crack width and b) median crack width.
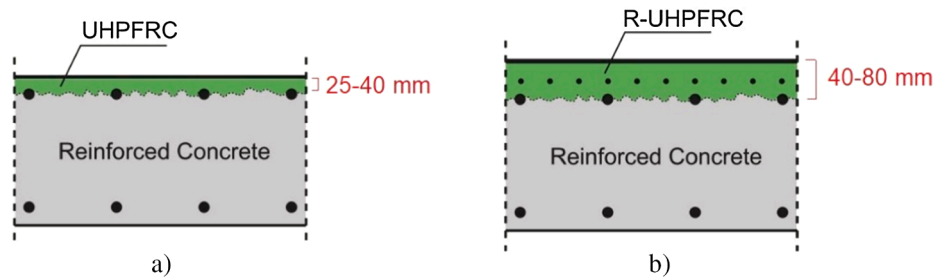
Fig. 17. Configuration of composite structural elements combining R-UHPFRC and conventional RC: a) UHPFRC layer (thickness 25–40 mm) has a protective function only; b) R-UHPFRC layer (thickness of 40–80 mm or more) has both structural resistance and protective features [57].

3.3. Chloride penetration

3.3.1. Visual analysis

All specimens were in excellent condition after the chloride cycles with no evidence of surface scaling, material loss or additional cracking, which corroborates previous findings [32]. However, corrosion on fibres close to the exposed surface was generally observed, as shown in Fig. 14. In fact, fibre located up to 3 mm from the exposed surface, usually suffers severe corrosion. On the other hand, those fibres fully embedded inside of the concrete, remained free from corrosion [49–51].

3.3.2. Chloride penetration depth and chlorides profile analysis

After cutting and removing powder on the specimen surface, a 0.1 M silver nitrate solution was sprayed on one of the cut sections. Visible white silver chloride precipitation indicates the chloride penetration depth, which can be seen in Appendix C, namely, Figs. 19–21, for 3.0%-300-i, 3.0%-350-i 3.0%-400-i, respectively. It must be noted that some reaction occurred between the fibres and the silver nitrate solution, which is perceived in Figures of Appendix C. Detailed results of penetration depth regarding each specimen is presented in Table 7 in Appendix B.

For cracked specimens, two regions of chloride penetration depth could be distinguished, the penetration in the non-cracked zone (D_m) and the penetration in the main crack zone (D_{crack}), as indicated in Fig. 7 on section 2.7. D_{crack} was located where a macro-crack was found in between the two loading points. In the cracked specimens (3.0%-350-i and 3.0%-400-i), a localised and significant chloride penetration (between 10 and 17 mm) was observed close to the macro-crack. On the other hand, more uniform penetration occurred in reference specimens or healthy areas of cracked specimens (roughly 2–3 mm).

Concerning loaded-cracked specimens, 3.0%-300-i, a different chloride penetration pattern was observed, since these specimens present mainly micro-cracking, instated of an evident macro-crack as observed in series 3.0%-350-i and 3.0%-400-i. These micro-cracks promoted suction of aqueous chloride solution, giving rise to small penetration through them, as can be seen in Fig. 19 of Appendix C. The maximum chloride penetration depth was 18–19 mm, while in the non-cracked zone was 2 mm. It must be noted that, in 3.0%-300-i specimens, some chloride condensation occurred in the loaded surface of the specimens (see Fig. 19 of Appendix C), since it was not possible to protect this surface with the waterproof tape.

Fig. 15 presents the chloride profiles and chloride content values for each specimen at different depths (detailed data can be found in Table 7 of Appendix B). The chloride content is expressed as the percentage of chloride ions by mass of the sample (without steel fibres – UHPC). Fig. 15 also depicts the C_0 (blue line in Fig. 15-a, b, c and d).

The non-cracked specimens (3.0%-0-i) showed a high chloride concentration close to the specimens surface, decreasing towards the specimens inner. These results are in agreement with the colourimetric analysis with silver nitrate. The maximum chloride content varied between 0.47 and 0.79% at a depth ranging from 0 to 5 mm, then, between 5 and 10 mm depth, the chloride content drastically decreased (around 50%) for values between 0.26% and 0.41%, see Fig. 15-a. Afterwards, chloride profiles kept decreasing with an asymptotic shape converging to 0.20% as depicted in Fig. 15-a.

On cracked specimens, samples taken near a macro-crack and non-cracked areas were analysed and depicted in Fig. 15-b, -c and -d, using full and dashed lines, respectively (chloride profiles data is also compiled in Table 7 of Appendix B). Generally, chlorides profiles appear to be similar despite the different COD_{load} applied. In fact, on cracked-unloaded specimens, 3.0%-350-i and 3.0%-400-i, the chlorides could penetrate inwards more rapidly due to the induced macro-crack.

Target COD_load = 350 μm

	1	2	3	4
A	61 7 28 11	6		4
B	102 20 11 6		5	
C	6 41	110		

	1	2	3	4
A	7 5 7 58	4		4
B	5 11			52
C			3 64	

	1	2	3	4
A	12			8 36 117 92
B	4	3	4 52 50 73 14 14	7 44
C	4 6	5 6 39 111	76 35	3

Target COD_load = 400 μm

	1	2	3	4
A	206 13	12 4		3
B	4	98 94 16	3 2	2 2
C	79	129	2	

	1	2	3	4
A	3 3		28 37 28 36 3	5 3 2 20
B	3 3 2		65 48 8	36 23
C	2		2	3 58 60 18 25

	1	2	3	4
A	3			212 18 17 6
B			47 179 5	
C	3		163 7	26

Legend:
- 0 – 50 μm
- 51 – 100 μm
- 101 – 200 μm
- > 200 μm
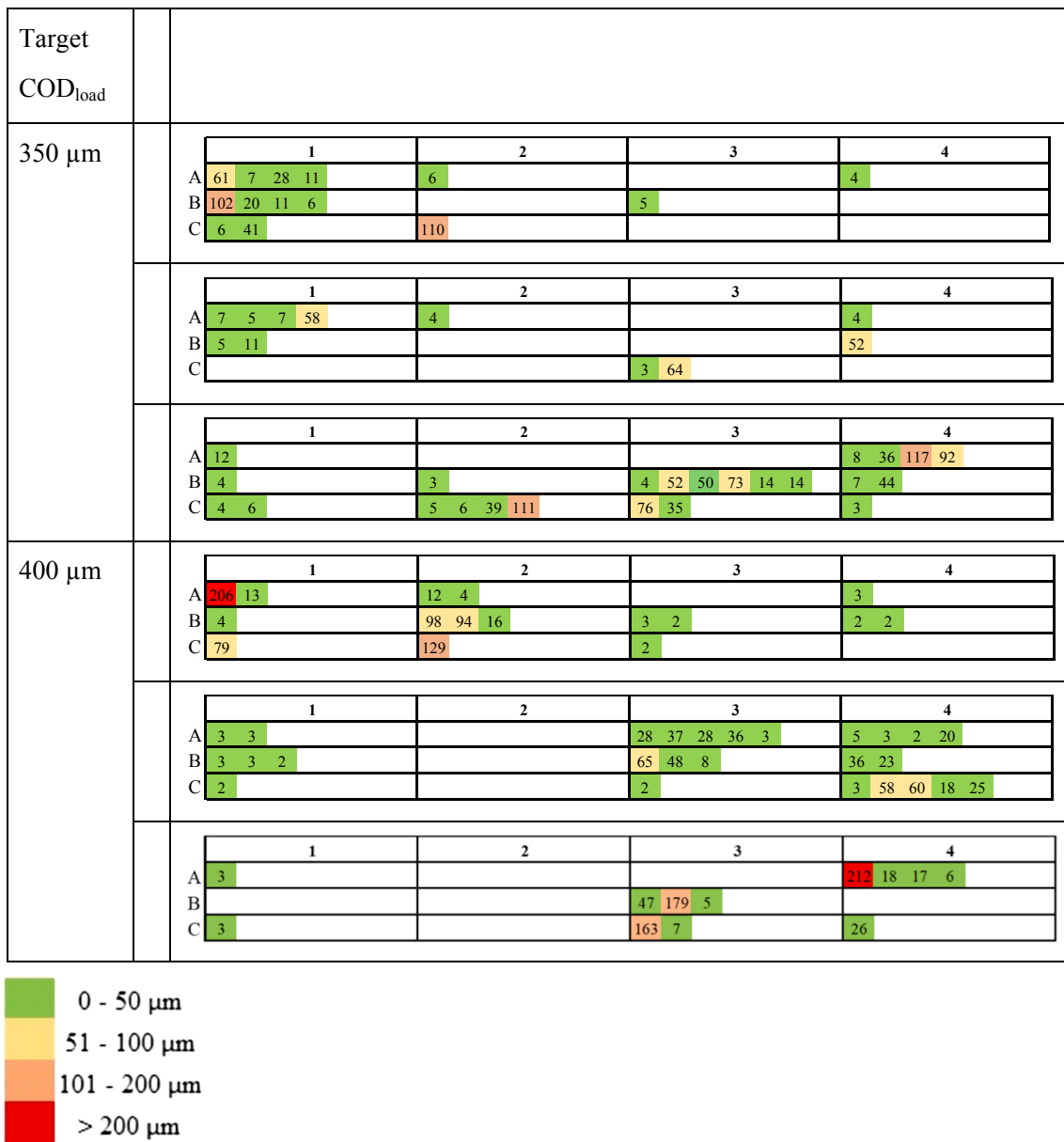
Fig. 18. Localisation of cracks observed in UHPFRC specimens nd corresponding crack widths (in μm).

Maximum chloride content takes place close to the surface and then decreases as the penetration depth increases. The maximum chloride content, near the surface, varied between 0.61 and 0.98% and 0.62–0.90% for 3.0%-350-i and 3.0%-400-i specimens, respectively. Regarding the non-cracked area, maximum chloride content, near the surface, was 0.84% and 0.80% for 3.0%-350-i and 3.0%-400-i specimens, respectively. The main difference between crack and the non-cracked area is that the chloride content drastically reduced after 5 mm from the surface of specimens and it keeps nearly constant up to 20 mm depth. These findings corroborate with colourimetric analysis with silver nitrate, in which penetration front is different in non-cracked and cracked areas (see Appendix C, Figs. 19–21, for 3.0%-350-i 3.0%-400-i, respectively).

As can be observed in Fig. 16 -b, it seems higher median crack width gave rise to higher chloride content. On the other hand, chloride content did not show any tendency regarding maximum crack width, as shown in Fig. 16-a. This seems to make sense since up to a particular value of crack width, the suction capacity should be dominant. It should be noted that it is common practice to discard the first mm of a chloride profile

sample and take the next increment, around the 10 mm depth, as a constant initial, pseudo surface concentration [52], thus Fig. 16 illustrates results of chloride content concerning only 5–10 mm depth.

On cracked-loaded specimens, "3.0%-300-i ", the maximum chloride content in the cracked area was 0.61–0.65%. After 138 days of chloride cycles, the cracked zones chloride concentration was similar and varied between 0.43 and 0.62%. The 3.0%-300-i specimens presented also improved behaviour in terms of resistance to ingress of chlorides, compared to the remaining cracked specimens, which the occurrence of self-healing might explain. After the first wetting–drying cycles the fine micro-cracks sealed, which slowed the chlorides ingress. These results are in agreement with the bending test results previously discussed section 3.3.2.

3.3.3. Critical chloride content and UHPFRC cover

The critical chloride content (Ccrit) is commonly defined as the chloride content at the steel depth necessary to sustain local passive film breakdown and initiate the corrosion process [53]. The critical chloride content is often referred to as the percentage of the cement content.

Specimen	3.0%-300-i
3.0%-300	
3.0%-300	

Fig. 19. Chlorides ingress of 3.0%-300-i specimens (penetration depth of chloride ions in lighter part).

Specimen	3.0%-350-i
3.0%-350-4	
3.0%-350-5	
3.0%-350-6	
3.0%-350-8	
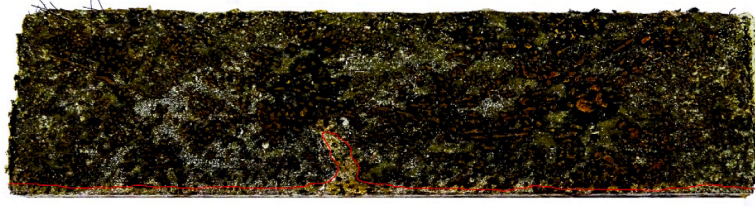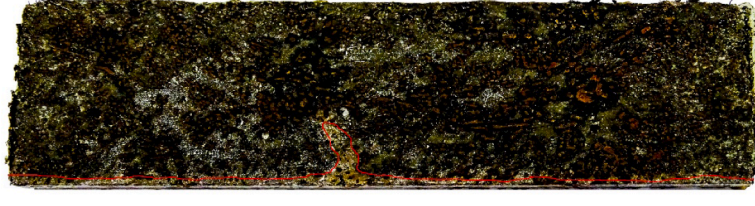
Fig. 20. Chlorides ingress of 3.0%-350-i specimens (penetration depth of chloride ions in lighter part).

Specimen	3.0%-400-i
3.0%-400-3	
3.0%-400-4	
3.0%-400-5	
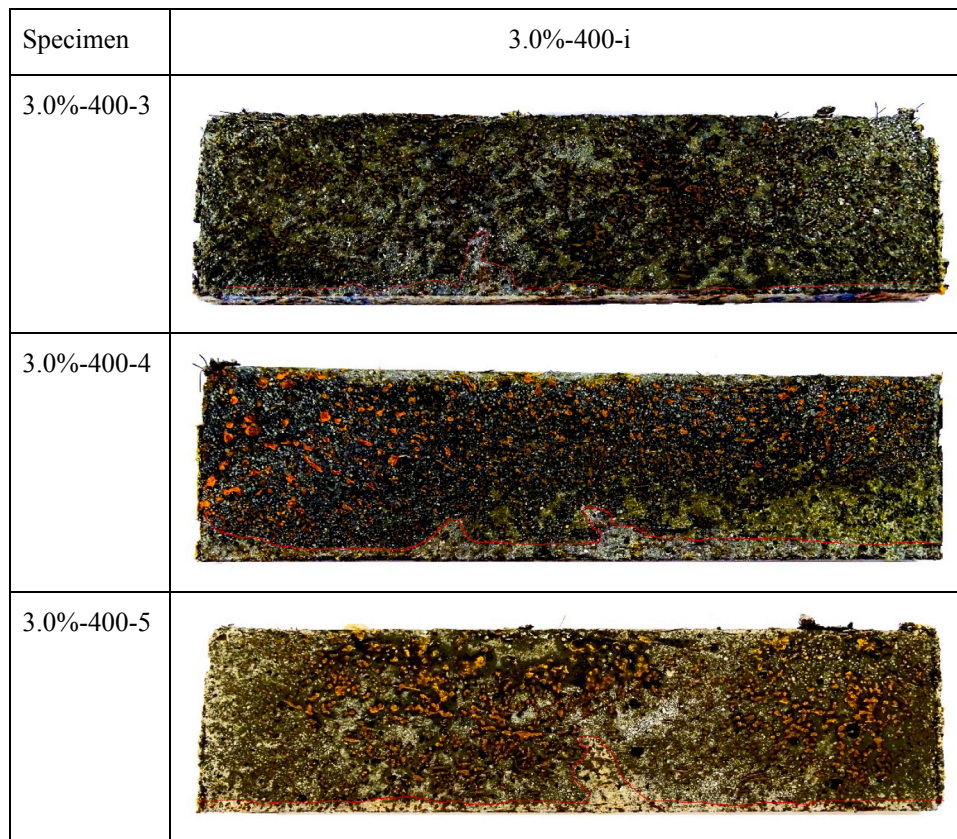
Fig. 21. Chlorides ingress of 3.0%-400-i specimens (penetration depth of chloride ions in lighter part).

Different authors have reported different chloride thresholds to depassivate the reinforcing steel [54,55]. International standards present limits on the tolerable chloride content in cement-based composites. For example, the European standard NP EN 206–1 [56] restricts the chloride content to 0.40% by mass of binder for reinforced concrete structures. The Ccrit suggested in NP EN 206–1 [56] is depicted in Fig. 15, red lines. It should be noted that Ccrit = 0.40% corresponds to the mass of cement plus type II additions, thus this limit needed to be converted in terms of the mass of UHPC, the result being Ccrit = 0.16%.

Non-cracked specimens (Fig. 15-a) presented significant chloride content, higher than Ccrit = 0.16% up to 20 mm depth. Regarding non-cracked areas of cracked series specimens, 3.0%-300-i, 3.0%-350-i and 3.0%-400-i, the surface chloride content (considering 5–10 mm [52]), was about 0.16% of UHPC mass (Fig. 15-b, -c and -d). On the other hand, chloride content assessed on the main (and visible) crack revealed that up to a depth of 20 mm the chloride content was above 0.16%. Though, it shows a decreasing tendency for higher depths.

Based on these experimental campaign results, one can conclude that a minimum of 20 mm cover to reinforcement might be necessary to avoid rebar corrosion. This would be feasible considering the typical thickness of new reinforced UHPFRC layers, of 40–80 mm, as suggested in Fig. 17 [57].

Nevertheless, it should be pointed that: i) these Ccrit value suggested in NP EN 206–1 is not a proper chloride threshold value, but rather a practical limit value for the production of fresh concrete [55]; ii) wetting and drying cycles in a laboratory environment can be more severe than "in-situ" exposure due to ambience (temperature, humidity, carbonation, seawater composition) and scale factors. These can also be concluded from comparing the results of "in situ" campaign performed by Thomas et al. [32] and the remaining works reported in section 1.2. The chloride content after 5–15 years on field [32] were similar to those obtained in (faster) laboratory experiments [34–36]. Field experiments are preferred when studying this topic, but these are very time-

consuming and often unfeasible, taking into account a PhD project duration. However, they can play an essential role in checking or calibrating laboratory results.

4. Conclusions

The present research aimed to evaluate the effect of cracking and loading conditions on the chloride penetration in a UHPFRC recently developed by the authors. Thus, an experimental campaign was performed in which UHPFRC specimens were kept in a chloride rich environment for one year. Several parameters were evaluated, including mechanical performance, chloride penetration depth, chloride content, crack pattern characterisation. The following conclusions were drawn:

- Cracking recover:
  - After unloading the UHPFRC specimens, a COD recovery occurred. Residual COD, $COD_{res,}$ oscillated between 132 and 243 μmand exists a linear relationship between COD_{res} and COD_{load}Up to a COD_{res} of about 200 μm, the maximum crack width remained below 75 μm. A more significant increase in maximum crack width (>200 μm) was observed for higher COD_{res}.
- Mechanical properties after chloride exposure:
  - Loaded and micro-cracked specimens, 3.0%-300-i, exposed to chloride cycles, presents a quasi-total recovery of their initial stiffness, as well as no loss of flexural strength.
  - Cracked-unloaded specimens, 3.0%-350-i and 3.0%-400-i, had a considerable loss of initial stiffness, while flexure strength was not significantly affected.
  - The improved behaviour of the "3.0%-300-i" specimens can be explained by the lower damage imposed to these specimens, leading to the formation of only fine micro-cracks. Contrarily, in the case of "3.0%-350-i" and "3.0%-400-i" specimens, a macro-crack has formed, which could not be completely sealed by the

autogenous healing, thus causing an irreversible decrease in the initial stiffness.

- Chloride penetration:
  - All specimens were in excellent condition with no evidence of surface scaling or additional cracking after long term chloride exposure, but corrosion of fibres closer to the surface was observed, as expected;
  - A penetration depth of approximately 10–17 mm was found on the cracks surrounding area. However, in non-cracked regions, about 2–3 mm, the penetration depth was similar to the penetration over non-cracked specimens (3.0%-0-i).
  - The maximum chloride content, between 5 and 10 mm depth, and on crack area, varied between 0.41 and 0.60% and 0.49–0.55%for 3.0%-350-i and 3.0%-400-i specimens, respectively.
  - On cracked-loaded specimens, 3.0%-300-i, the maximum chloride content on the cracked area was 0.38–0.46%.
  - The main difference between crack and the non-cracked area is that the chloride content drastically reduced after 5 mm from the surface of specimens and it keeps nearly constant up to 20 mm depth.
  - Chloride contents observed in these experimental campaigns, up to 20 mm depth, were superior to Ccrit = 0.16% by mass of UHPC, particularly near the macro-crack of specimens 3.0%-350-i" and "3.0%-400-i".

Based on these campaign results only, a UHPFRC cover of at least 20 mm would be recommended for exposure classes XS3 to protect a concrete substrate in hybrid structures. However, it should be considered that accelerated test in the laboratory can be more severe than the exposure of real structures to natural ambient conditions. Thus, real field tests would be necessary to calibrate laboratory results.

CRediT authorship contribution statement

Ana Mafalda Matos: Conceptualization, Methodology, Formal analysis, Investigation, Writing – original draft, Writing – review & editing. **Stefan Chaves Figueiredo:** Conceptualization, Methodology, Investigation, Writing – review & editing. **Sandra Nunes:** Writing – review & editing, Supervision, Funding acquisition, Project administration. **Erik Schlangen:** Writing – review & editing, Supervision, Funding acquisition, Project administration. **José L. Barroso Aguiar:** Writing – review & editing, Supervision, Funding acquisition.

Declaration of Competing Interest

The authors declare that they have no known competing financial interests or personal relationships that could have appeared to influence the work reported in this paper.

Acknowledgements

Appendix A

(See Fig. 18)

Appendix B

(See Tables 6 and 7)

Appendix C

(See Figs. 19–21)

References

[1] S. Abbas, M.L. Nehdi, M.A. Saleem, Ultra-high performance concrete: mechanical performance, durability, sustainability and implementation challenges, Int. J. Concr. Struct. Mater. 10 (3) (2016) 271–295, https://doi.org/10.1007/s40069-016-0157-4.

[2] F. Toutlemonde, M. Carcasses, M. Lion, Field Experience of UHPFRC Durability in an Air Cooling Tower, n.d. https://www.scopus.com/record/display.uri?eid=2-s2.0-84974672568&origin=inward&txGid=3BE2BB6FD715C5189C394FB0BF7AF952.wsnAw8kcdt7IPYLO0V48gA%3A133.

[3] J. Provete Vincler, T. Sanchez, V. Turgeon, D. Conciatori, L. Sorelli, A modified accelerated chloride migration tests for UHPC and UHPFRC with PVA and steel fibers, Cem. Concr. Res. 117 (2019) 38–44, https://doi.org/10.1016/J.CEMCONRES.2018.12.006.

[4] E. Denarie, E. Bruhwiler, Cast-on site UHPFRC for improvement of existing structures – achievements over the last 10 years in practice and research, in: 7th work. High Perform. Fiber Reinf. Cem. Compos., Stuttgart, Germany, 2015. https://infoscience.epfl.ch/record/215013/files/HPFRCC7_2015_ED_EB.pdf. Accessed June 11, 2017.

[5] E. Brühwiler, Rehabilitation and strengthening of concrete structures using ultra-high performance fibre reinforced concrete, Concr. Repair, Rehabil. Retrofi Tting III. (2012).

[6] Z. Zhou, P. Qiao, Durability of ultra-high performance concrete in tension under cold weather conditions, Cem. Concr. Compos. 94 (2018) 94–106, https://doi.org/10.1016/J.CEMCONCOMP.2018.08.019.

[7] W. Wang, J. Liu, F. Agostini, C.A. Davy, F. Skoczylas, D. Corvez, Durability of an ultra high performance fiber reinforced concrete (UHPFRC) under progressive aging, Cem. Concr. Res. 55 (2014) 1–13, https://doi.org/10.1016/J.CEMCONRES.2013.09.008.

[8] N. Van Tuan, G. Ye, K. van Breugel, A.L.A. Fraaij, D.D. Bui, The study of using rice husk ash to produce ultra high performance concrete, Constr. Build. Mater. 25 (4) (2011) 2030–2035, https://doi.org/10.1016/j.conbuildmat.2010.11.046.

[9] V. Vaitkevičius, E. Šerelis, H. Hilbig, The effect of glass powder on the microstructure of ultra high performance concrete, Constr. Build. Mater. 68 (2014) 102–109, https://doi.org/10.1016/j.conbuildmat.2014.05.101.

[10] S. Pyo, H.-K. Kim, Fresh and hardened properties of ultra-high performance concrete incorporating coal bottom ash and slag powder, Constr. Build. Mater. 131 (2017) 459–466, https://doi.org/10.1016/J.CONBUILDMAT.2016.10.109.

[11] S.H. Chu, Development of infilled cementitious composites (ICC), Compos. Struct. 267 (2021) 113885, https://doi.org/10.1016/j.compstruct.2021.113885.

[12] G. Habert, E. Denarié, A. Šajna, P. Rossi, Lowering the global warming impact of bridge rehabilitations by using ultra high performance fibre reinforced concretes, Cem. Concr. Compos. 38 (2013) 1–11, https://doi.org/10.1016/J.CEMCONCOMP.2012.11.008.

[13] B. Graybeal, E. Brühwiler, B.-S. Kim, F. Toutlemonde, Y.L. Voo, A. Zaghi, International perspective on UHPC in bridge engineering, J. Bridg. Eng. 25 (11) (2020) 04020094, https://doi.org/10.1061/(ASCE)BE.1943-5592.0001630.

[14] M.D. McDonagh, A.J. Foden, P.J. Brinckerhoff Andrew Foden, P. Brinckerhoff, Benefits of Ultra-High Performance Concrete for the Rehabilitation of the Pulaski Skyway, n.d.

[15] K. Zmetra, A.E. Zaghi, K. Wille, Rehabilitation of steel bridge girders with corroded ends using ultra-high performance concrete, Struct. Congr. 2015 – Proc. 2015 Struct. Congr. (2015) 1411–1422. doi:10.1061/9780784479117.121.

[16] E. Brühwiler, E. Denarié, Rehabilitation and strengthening of concrete structures using ultra-high performance fibre reinforced concrete, Struct. Eng. Int. 23 (4) (2013) 450–457, https://doi.org/10.2749/101686613X13627347100437.

[17] N. Randl, T. Steiner, S. Ofner, E. Baumgartner, T. Mészöly, Development of UHPC mixtures from an ecological point of view, Constr. Build. Mater. 67 (2014) 373–378, https://doi.org/10.1016/j.conbuildmat.2013.12.102.

[18] P. Racky, Cost-effectiveness and sustainability of UHPC, in: Int. Symp. Ultra High Perform. Concr., Kassel, Germany, 2004, pp. 797–805.

[19] K.H. Khayat, M. Valipour, Final Report Prepared for Missouri Department of Transportation Design and Performance of Cost-Effective Ultra High Performance Concrete for Bridge Deck Overlays, 2018. https://orcid.org/0000-0003-1431-0715. Accessed April 26, 2018.

[20] M. Kunieda, K. Asai, K. Sasaki, Cracking resistance of UHPFRC for repair application, Bridg. Maint. Saf. Manag. Life Cycle Sustain. Innov. (2021) 2805–2809, https://doi.org/10.1201/9780429279119-382.

[21] K. Wille, A.E. Naaman, Pullout behavior of high-strength steel fibers embedded in ultra-high-performance concrete, ACI Mater. J. 109 (2012) 479–488, https://doi.org/10.14359/51683923.

[22] K. Wille, A.E. Naaman, Effect of ultra-high-performance concrete on pullout behavior of high-strength brass-coated straight steel fibers, ACI Mater. J. 110 (2013) 451–462, https://doi.org/10.14359/51685792.

[23] A. Abrishambaf, M. Pimentel, S. Nunes, Influence of fibre orientation on the tensile behaviour of ultra-high performance fibre reinforced cementitious composites, Cem. Concr. Res. 97 (2017) 28–40, https://doi.org/10.1016/J.CEMCONRES.2017.03.007.

[24] S. Ahmad, I. Hakeem, M. Maslehuddin, Development of UHPC mixtures utilising natural and industrial waste materials as partial replacements of silica fume and sand, Sci. World J. (2014), https://doi.org/10.1155/2014/713531.

[25] M. Alkaysi, S. El-Tawil, Z. Liu, W. Hansen, Effects of silica powder and cement type on durability of ultra high performance concrete (UHPC), Cem. Concr. Compos. 66 (2016) 47–56, https://doi.org/10.1016/j.cemconcomp.2015.11.005.

[26] A. Tafraoui, G. Escadeillas, T. Vidal, Durability of the ultra high performances concrete containing metakaolin, Constr. Build. Mater. 112 (2016) 980–987, https://doi.org/10.1016/j.conbuildmat.2016.02.169.

[27] S. Abbas, A.M. Soliman, M.L. Nehdi, Exploring mechanical and durability properties of ultra-high performance concrete incorporating various steel fiber lengths and dosages, Constr. Build. Mater. 75 (2015) 429–441, https://doi.org/10.1016/j.conbuildmat.2014.11.017.

[28] D. Wang, C. Shi, Z. Wu, J. Xiao, Z. Huang, Z. Fang, A review on ultra high performance concrete: part II. Hydration, microstructure and properties, Constr. Build. Mater. 96 (2015) 368–377, https://doi.org/10.1016/j.conbuildmat.2015.08.095.

[29] A.M. Matos, S. Nunes, C. Costa, J.L. Barroso-Aguiar, Spent equilibrium catalyst as internal curing agent in UHPFRC, Cem. Concr. Compos. 104 (2019) 103362, https://doi.org/10.1016/j.cemconcomp.2019.103362.

[30] R. Wang, X. Gao, Q. Li, Y. Yang, Influence of splitting load on transport properties of ultra-high performance concrete, Constr. Build. Mater. 171 (2018) 708–718, https://doi.org/10.1016/J.CONBUILDMAT.2018.03.174.

[31] J. Li, Z. Wu, C. Shi, Q. Yuan, Z. Zhang, Durability of ultra-high performance concrete – a review, Constr. Build. Mater. 255 (2020) 119296, https://doi.org/10.1016/j.conbuildmat.2020.119296.

[32] M. Thomas, B. Green, E. ONeal, V. Perry, S. Hayman, A. Hossack, Marine performance of UHPC at Treat Island, in: 3rd Int. Symp. UHPC Nanotechnol. High Perform. Constr. Mater., Kassel Univ. Press, Kassel, Germany, 2012.

[33] G.U. Chunping, W. Qiannan, L. Jintao, S. Wei, The effect of nano-TiO2 on the durability of ultra-high performance concrete with and without a flexural load, Ceram.-Silik. 62 (2018) 374–381, https://doi.org/10.13168/cs.2018.0033.

[34] Z. Ma, T. Zhao, X. Yao, Influence of applied loads on the permeability behavior of ultra high performance concrete with steel fibers, J. Adv. Concr. Technol. 14 (12) (2016) 770–781, https://doi.org/10.3151/jact.14.770.

[35] F.H. Wittmann, X. Yao, P. Wang, P. Zhang, T. Zhao, Influence of an imposed tensile stress and subsequent self-healing on capillary absorption and chloride penetration into HPFRCC, in: High Perform. Fiber Reinf. Cem. Compos., RILEM, 2015, pp. 243–250.

[36] E. Parant, R. Pierre, F.L. Maou, Durability of a multiscale fibre reinforced cement composite in aggressive environment under service load, Cem. Concr. Res. 37 (7) (2007) 1106–1114, https://doi.org/10.1016/j.cemconres.2006.02.021.

[37] N. El-Joukhadar, S.J. Pantazopoulou, Effectiveness of UHPFRC cover in delaying bar corrosion, Constr. Build. Mater. 269 (2021) 121288, https://doi.org/10.1016/j.conbuildmat.2020.121288.

[38] E. Cuenca, S. Rigamonti, E. Gastaldo Brac, L. Ferrara, Crystalline admixture as healing promoter in concrete exposed to chloride-rich environments: experimental study, J. Mater. Civ. Eng. 33 (3) (2021) 04020491, https://doi.org/10.1061/(ASCE)MT.1943-5533.0003604.

[39] E. Cuenca, L. D'Ambrosio, D. Lizunov, A. Tretjakov, O. Volobujeva, L. Ferrara, Mechanical properties and self-healing capacity of ultra high performance fibre

[40] reinforced concrete with alumina nano-fibres: tailoring ultra high durability concrete for aggressive exposure scenarios, Cem. Concr. Compos. 118 (2021) 103956, https://doi.org/10.1016/j.cemconcomp.2021.103956.

[40] E. Cuenca, P. Serna, Autogenous self-healing capacity of early-age ultra-high-performance fiber-reinforced, Concrete 13 (6) (2021) 3061, https://doi.org/10.3390/su13063061.

[41] E. Cuenca, A. Mezzena, L. Ferrara, Synergy between crystalline admixtures and nano-constituents in enhancing autogenous healing capacity of cementitious composites under cracking and healing cycles in aggressive waters, Constr. Build. Mater. 266 (2021) 121447, https://doi.org/10.1016/j.conbuildmat.2020.121447.

[42] A.M. Matos, S. Nunes, C. Costa, J.L. Barroso-Aguiar, Characterisation of non-proprietary UHPC for use in rehabilitation/strengthening applications, in: V. Mechtcherine, K. Khayat, E. Secrieru (Eds.), RILEM Bookseries, Springer Netherlands, 2020, pp. 552–559. doi: 10.1007/978-3-030-22566-7_64.

[43] A.M. Matos, S. Nunes, José L. Barroso-Aguiar, C. Costa, Durabilidade de um material cimentício de ultraelevado desempenho reforçado com fibras metálicas, in: BETÃO ESTRUTURAL – BE2018, 2018.

[44] A.M. Matos, S. Nunes, J.L.B. Aguiar, Capillary transport of water in cracked and non-cracked UHPFRC specimens, J. Adv. Concr. Technol. 17 (5) (2019) 244–259, https://doi.org/10.3151/jact.17.244.

[45] Instituto Português da Qualidade, NP EN 197-1, Cement. Part 1: Composition, specifications and conformity criteria for common cements, (2012) 1–34.

[46] M.A. Vennesland, C. Climent, Andrade, Recommendation of RILEM TC 178-TM. Testing and modelling chloride penetration in concret.Methods for obtaining dust samples by means of grinding concrete in order to determine the chloride concentration profile, Mater. Struct. Constr. 46 (2013) 337–344, https://doi.org/10.1617/s11527-012-9968-1.

[47] IPQ, NP EN 196-2, Methods of testing cement – part 2: chemical analysis of cement, (2014) 80.

[48] D.-Y. Yoo, J.-H. Lee, Y.-S. Yoon, Effect of fiber content on mechanical and fracture properties of ultra high performance fiber reinforced cementitious composites, Compos. Struct. 106 (2013) 742–753, https://doi.org/10.1016/J.COMPSTRUCT.2013.07.033.

[49] A.M. Matos, S.C. Figueiredo, S. Nunes, E. Schlangen, Durability of fibre reinforced cementitious composites: coupling mechanical and chloride environment loads, in: G. Ye, Y. Yuan, C.R. Rodriguez, H. Zhang, B. Šavija (Eds.), 72nd RILEM Annu. Week SLD4 Conf. CONMOD2018 Symp, RILEM Publications SARL, Delft, The Netherlands, 2018, pp. 721–732.

[50] C.G. Berrocal, L. Karin, L. Ingemar, Influence of steel fibres on corrosion of reinforcement in concrete in chloride environments: a review, in: FIBRE Concr. 2013, Prague, Czech Republic, 2013. http://publications.lib.chalmers.se/records/fulltext/187376/local_187376.pdf. Accessed March 14, 2018.

[51] J.-L. Granju, S. Ullah Balouch, Corrosion of steel fibre reinforced concrete from the cracks, Cem. Concr. Res. 35 (3) (2005) 572–577, https://doi.org/10.1016/j.cemconres.2004.06.032.

[52] J.P. Broomfield, Corrosion of steel in concrete. Understanding, Investigation and Repair, 2nd ed.,, Taylor & Francis, 1997.

[53] K.Y. Ann, H.-W. Song, Chloride threshold level for corrosion of steel in concrete, Corros. Sci. 49 (11) (2007) 4113–4133, https://doi.org/10.1016/j.corsci.2007.05.007.

[54] C. Alonso, C. Andrade, M. Castellote, P. Castro, Chloride threshold values to depassivate reinforcing bars embedded in a standardised OPC mortar, Cem. Concr. Res. 30 (2000) 1047–1055, https://doi.org/10.1016/S0008-8846(00)00265-9.

[55] U. Angst, B. Elsener, C.K. Larsen, Ø. Vennesland, Critical chloride content in reinforced concrete – a review, Cem. Concr. Res. 39 (12) (2009) 1122–1138, https://doi.org/10.1016/j.cemconres.2009.08.006.

[56] C. Andrade, Future trends in research on reinforcement corrosion, in: Corros. Steel Concr. Struct., Elsevier Inc., 2016, pp. 269–288. doi: 10.1016/B978-1-78242-381-2.00014-6.

[57] K. Wassmann, E. Brühwiler, P. Lunk, Strengthening of RC slabs using UHPFRC – concepts and applications, in: 4th Int. Symp. Ultra-High Perform. Concr. High Perform. Mater., Kassel, Germany, 2016.

[58] A.M. Matos, S. Nunes, C. Costa, J.L.B. Aguiar, Durability of an UHPC containing spent equilibrium catalyst, Constr. Build. Mater. 305 (2021) 124681.